Binary Radio Pulsars
ASP Conference Series, Vol. 328, 2005
F. A. Rasio and I. H. Stairs

Probing Relativistic Winds: The Case of PSR J0737−3039 A and B

Jonathan Arons[1], D. C. Backer[1], Anatoly Spitkovsky[2], V. M. Kaspi[3]

[1] *University of California, Berkeley, Department of Astronomy, 601 Campbell Hall, Berkeley, CA 94720-3411*
[2] *Stanford University, Kavli Institute of Particle Astrophysics and Cosmology, P.O.Box 20540, MS 29, Stanford, CA 94309*
[3] *McGill University, Department of Physics, Montreal, QC H3A 2T8, Canada*

Abstract. We propose synchrotron absorption in a magnetosheath forming a cocoon around the magnetosphere of pulsar **B** to be the origin of the eclipse phenomena seen in the recently discovered double pulsar system PSR J0737−3039 **A** & **B**. The magnetosheath enfolds the magnetosphere of pulsar **B**, where the relativistic wind from **A** collides with **B**'s magnetic field. If this model is correct, it predicts the eclipses will clear at frequencies higher than those of the observations reported to date (nominally, above $\nu \sim 5\,\mathrm{GHz}$). The model also predicts synchrotron emission at the level of a few to $10\,\mu\mathrm{Jy}$, peaking at $\nu \sim 2 - 5\,\mathrm{GHz}$ with possible orbital modulation. We use simplified semi-analytic models to elucidate the structure of the **B** magnetosphere, showing that the **A** wind's dynamic pressure confines **B**'s magnetic field to within a radius less than 50,000 km from **B**, smaller than **B**'s light cylinder radius, on the "daytime" side (the side facing **A**). Downstream of **B** ("nighttime"), **B** forms a magnetotail. We use particle-in-cell simulations to include the effects of magnetospheric rotation, showing that the magnetosheath has an asymmetric density distribution which may be responsible for the observed eclipse asymmetries. We use simple estimates based upon the magnetic reconnection observed in the simulations to derive a "propellor" spindown torque on **B**, which is the dominant mode of angular momentum extraction from this star. Application of this torque to **B**'s observed spindown yields a polar dipole field $\sim 7 \times 10^{11}\,\mathrm{Gauss}$ (magnetic moment $\mu_B \sim 3.5 \times 10^{29}$ cgs). This torque has a braking index of unity. We show that the model can explain the known eclipses only if the **A** wind's density is at least 4 orders of magnitude greater than is expected from existing popular models of pair creation in pulsars. We discuss the implications of this result for our general understanding of pulsar physics.

Our proposal was qualitatively outlined in Kaspi et al. (2004) and Demorest et al. (2004). Since those papers' appearance, a similar proposal has been made by Lyutikov (2004).

1. Introduction

Rotation Powered Pulsars (RPPs) lose their rotational energy because of electromagnetic torques. While this fact has been known since the earliest days of pulsar research (Gold 1968; Goldreich & Julian 1969; Ostriker & Gunn 1969),

and indeed was predicted before pulsars' discovery (Pacini 1967), (1) the physics of the processes through which the extraction works, (2) the physics of how the rotational energy is transmitted to the surrounding world, and (3) the physics of how that energy transforms into the observed synchrotron radiation from the nebulae around pulsars have all remained open questions. Answers to all three questions are of significance not only to the understanding of RPPs themselves, but also to the physics of Active Galactic Nuclei and to the workings of Gamma Ray Burst sources, especially if these outflows are driven by large scale Poynting fluxes from systematically magnetized disks (or perhaps magnetars, in the GRB case).

Modern pulsar theory suggests that a RPP throws off its rotational energy in the form of a relatively dense, magnetized relativistic plasma wind, largely composed of electron-positron pairs with an embedded wound up magnetic field. Particle acceleration in electrostatic "gaps" (polar cap gaps, outer gaps or slot gaps) is thought to be the origin of the $e^{\pm}$ plasma, through emission and conversion of gamma rays from accelerated particles within a RPP's magnetosphere (e.g., Hibschman & Arons 2001; Harding & Muslimov 1998; Muslimov & Harding 2003; Hirotani et al. 2003). The outflow densities suggested by these models justify the use of relativistic MHD in modeling the winds (e.g., Beskin, Kuznetsova & Rafikov 1998; Bogovalov 1999; Contopoulos, Kazanas & Fendt 1999; Vlahakis 2004). Theoretical models of MHD winds exhibit negligible radiative emission (by construction), and indeed, there has been no positive observational identification of the winds themselves — observational study of the winds' properties has depended on detection of the winds' consequences. The winds are like a river flowing on dark nights — invisible until the water strikes a dam, or rocks in the stream, when the glimmer of starlight from the spray thrown by the obstacles allows one to infer the river's presence and properties.

To date, the main useful probe of RPPs' energy flow has been the winds' collisions with the "dams" created by interstellar and circumstellar media surrounding RPPs. These collisions create prominent Pulsar Wind Nebulae (PWNe) around the young pulsars with large rates of rotational energy loss $\dot{E}_R = c\Phi^2$ (Φ is the electric potential drop across the magnetospheric open field lines). The radiative emissions from these nebulae allow inferences of the plasma content and magnetization at the winds' termination working surfaces (shock waves, in most interpretations). See Arons (1998, 2002, 2004), Slane (2002), Chevalier (2002, 2004), Reynolds (2003), Komissarov & Lyubarsky (2003), Spitkovsky & Arons (2004), and Del Zanna et al. (2004) for recent reviews and results on this class of interactions.

Rocks in the relativistic stream provide another window into relativistic wind behavior. Examples of such interactions are the collision between the wind and the "excretion" disk around the Be star in PSR 1263−59 (e.g., Kaspi et al. 1995; Johnston et al. 1996, 2001; Tavani & Arons 1997), and the collision of the wind from the millisecond pulsar PSR 1957+20 with the non-relativistic wind from its companion star (Fruchter et al. 1988; Ruderman et al. 1989; Arons & Tavani 1993). As with the PWNe, most of what has been gleaned about the wind properties has come from interpretations of the X-ray detections.

The recent discovery of the double pulsar system PSR J0737−3039 **A** & **B** (Burgay et al. 2003; Lyne et al. 2004) offers a new window into studying a relativistic wind, in this case through the tools of radio astronomy. The binary has an orbital period P_b of 2.4 hours, an orbital eccentricity $e = 0.08$ and an inclination angle 87 ± 3 degrees. Pulsar **A** has a spin period P_A of 22.7 ms, a rotational energy loss rate $\dot{E}_A$ of $0.6 \times 10^{34}\,\mathrm{erg\,s^{-1}}$, and a light cylinder radius $R_{\rm LA} = cP_A/2\pi$ =1,084 km, which is small compared to the orbit semi-major axis $a = (4.25 \pm 0.05) \times 10^5$ km. Pulsar **B** has a pulse period P_B of 2.77 s, spin-down rate $\dot{P}_B$ of $0.8 \times 10^{-15}\,\mathrm{s\,s^{-1}}$ which leads to a rotational energy loss rate $\dot{E}_B$ of $2 \times 10^{30}\,\mathrm{erg\,s^{-1}}$, and a light-cylinder radius $R_{\rm LB} = 1.32 \times 10^5$ km. Pulsar **A** shows a brief eclipse that lasts approximately 30 seconds when **A** passes behind **B** along the line of sight, at *inferior conjunction*[1]. This eclipse shows substantially slower ingress (7 s) than egress (4 s), and the full eclipse profile is nearly achromatic (Kaspi et al. 2004). The flux density and emission profile of pulsar **B** vary around the orbit in nearly achromatic manner over the range 430 MHz to 3.2 GHz (Lyne et al. 2004; Demorest et al. 2004; Ramachandran et al. 2004). The strongest emission episodes of **B** are during two orbital longitude ranges about 70° apart and asymmetrically spaced by $\sim 30°$ with respect to inferior conjunction. Two weak **B** emission episodes are located $\sim 115°$ before inferior conjunction (lasting $\sim 40°$) and 90° after inferior conjunction (lasting $\sim 60°$). Pulsar **B** is not detected, or perhaps is seen with pulsed flux at the level of $\sim 0.4\%$ of its maximum flux, during a range of orbital longitude that starts $\sim 60°$ before superior conjunction, and ends $\sim 30°$ after this epoch — effectively, this episode is an eclipse of **B**.

These eclipses and emission episodes of **B** offer an opportunity to probe the wind around **A** much closer to the energizing pulsar than has been possible using PWNe in higher voltage systems. Furthermore, the radio observations are sensitive to low energy relativistic electrons and positrons, providing a look into the instantaneous state of this component of a relativistic wind's plasma — PWNe observations only constrain their winds' low energy particle content averaged over the lives of the nebulae.

We propose that **B**'s magnetosphere has a structure more similar to that of the Earth's magnetosphere than to the magnetospheres of pulsars not interacting with a companion. In contrast, **A**'s magnetospheric properties are decoupled from the binary. Thus, the collision of **A**'s wind with **B**'s magnetosphere causes the formation of a bow shock. The pressure of the post-shock particles and fields confines the **B** magnetosphere on the side that instantaneously faces **A**, with a magnetotail extending behind **B**. Magnetic reconnection allows the shocked wind to create a tangential stress on **B**'s magnetosphere, which creates the dominant spin-down torque on **B** (a variant of the propellor effect). There is also a less significant relativistic wind component to the torque on **B**, created by wind from **B** flowing out the magnetotail, whose transverse size is comparable to $R_{\rm LB}$. We speculate that the propellor torque also includes components that

[1]This is standard terminology assuming that **A** is the *primary* star and **B** the *secondary*. Likely binary evolution scenarios suggest that this is the appropriate nomenclature for the two evolved remnants of the original main-sequence system. *Superior conjunction* occurs a half orbit later when **B** passes behind **A** along the sight line.

align **B**'s rotation axis with the orbital angular momentum. If so, **B** must be an orthogonal rotator, with its magnetic axis perpendicular to its spin axis.

Polarization observations obtained by Demorest et al. (2004) show that **A** is almost an aligned rotator (angle between **A**'s magnetic and rotation axes $\sim 5^\circ$), with its spin axis substantially misaligned with the orbital angular momentum, $\angle(\mathbf{\Omega}_A, \mathbf{\Omega}_{\rm orbit}) \sim 50^\circ$. Then the equatorial current sheet in **A**'s wind is likely to have thickness $\sim 10^\circ$ around the wind's equator, with the result that for 340° of orbital phase, **B** is immersed in the high latitude, possibly slow and dense $e^\pm$ wind. We suggest that latitudinal variation in the confining pressure exerted by the wind causes variation of **B**'s beaming morphology, which may be in part responsible for the orbit dependent variations of **B**'s pulse morphology.

The bow shock creates a magnetosheath of relativistic hot, magnetized plasma which enfolds the confined **B** magnetosphere. We show that synchrotron absorption in the magnetosheath can explain the eclipse of **A** at inferior conjunction and of **B** at superior conjunction. The model, which requires surprisingly high density in the **A** wind, predicts eclipse clearing at frequencies higher than observed to date — nominally, above 5 GHz — and also predicts observable, orbitally modulated synchrotron emission, at the level of $10\,\mu$Jy at $\nu \sim 5$ GHz.

In the context of this model the eclipses of **A** and **B** and the other emission phenomenology of **B** provide the first significant constraint on the properties of a relativistic wind near its source — **B** forms a magnetospheric rock in the relativistic stream from **A** only 785 light cylinder radii outside the fast pulsar's magnetosphere. The model suggests that σ, the ratio of Poynting flux to kinetic energy flux, in **A**'s wind just upstream of the bow shock is certainly less than 2.5 and probably ~ 0.2, much less than what is expected from existing ideal MHD theories of relativistic wind outflow. Thus, the interaction of **A**'s wind with **B** suggests magnetic dissipation in the wind begins quite close to the source.

2. Magnetospheric Shape and Torques

We follow geophysical practice and identify the direction from **B** to **A** as "noon" as seen from **B**, with "daytime" being the hemisphere facing **A**. The simulations described below show that the rotating magnetosphere develops polar cusps in the magnetic field as each pole rotates past noon, features which correspond to rotationally induced asymmetry of the magnetosheath. Using this asymmetry to interpret the asymmetry of the **A** eclipse suggests the **B** pulsar has prograde rotation with respect to the orbit, which identifies "dawn" and "dusk" as the directions parallel and antiparallel to B's orbital velocity, respectively. "Midnight" is in the downstream direction, looking down the magnetotail. Balancing the full relativistic dynamic pressure of **A**'s wind against **B**'s magnetic pressure yields a force balance radius at the magnetospheric apex on the daytime side

$$R_{m0} = \left(\frac{8\mu_B^2 a^2 c}{\dot{E}_A \sin^2\Theta_{AB}}\right)^{1/6} \simeq 4.84\times10^4 \left(\frac{\mu_{B,30}}{0.375}\csc\Theta_{AB}\right)^{1/3}\ {\rm km}, \qquad (1)$$

where μ_B is **B**'s magnetic moment, $\mu_{B,30} = \mu_B/10^{30}$ cgs and Θ_{AB} is the angle between **A**'s rotation axis and **B**'s orbital position - **A**'s wind has dynamic

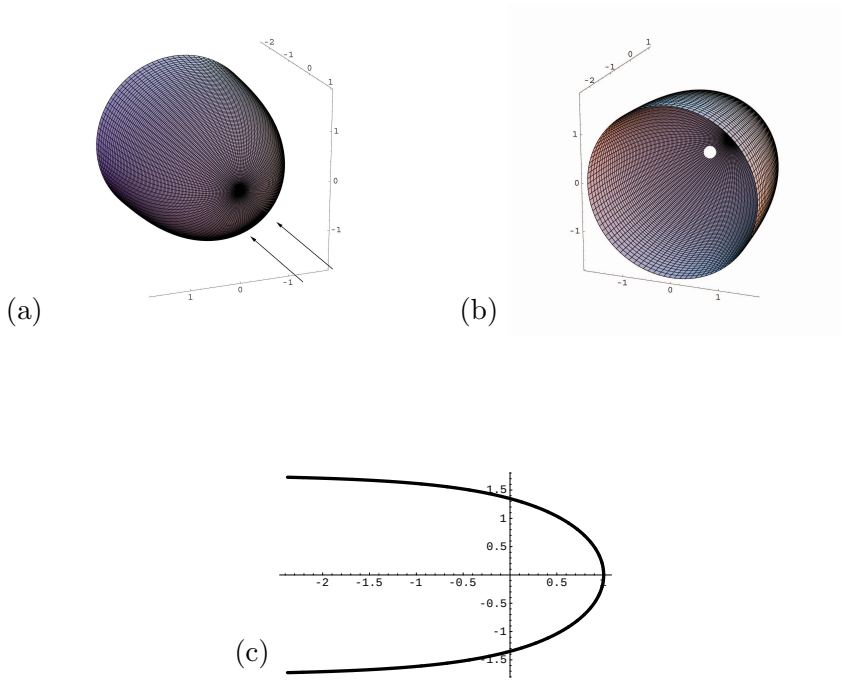

Figure 1. Shape of **B**'s magnetosphere, in a steady flow, axisymmetric pressure equilibrium model. (a) The magnetospheric obstacle as seen from upstream in **A**'s wind. (b) The magnetospheric obstacle as seen looking up the magnetotail. The **B** neutron star is the white dot (not to scale). (c) A cross section of the magnetopause surface, taken through the axis of symmetry. The magnetopause radius is measured in units of R_{m0}.

pressure varying with latitude. Since $\sin^2\Theta_{AB} = 1 - \sin^2 i_A \sin^2(\omega - \psi_A)$, the confining dynamic pressure varies by about a factor of two, twice during each orbit. Therefore the size of **B**'s daytime magnetosphere and its polar cap vary with orbital longitude ω. Here i_A is the angle between **A**'s angular velocity $\mathbf{\Omega_A}$ and the orbital angular momentum, probably $\sim 50^\circ$ (Demorest et al. 2004), and ψ_A is the angle between the projection of $\mathbf{\Omega_A}$ on the orbital plane and the line of apsides at $\omega = 0$.

Figure 1 shows the shape of a non-rotating **B** magnetosphere obtained from the pressure balance condition.

We have carried out a series of particle-in-cell (PIC) simulations of the **B** magnetosphere's structure, with **B**'s rotation included. Figure 2 shows snapshots, with **B** assumed to be an orthogonal rotator.

One can readily show that the tangential stress exerted by the reconnected field on the rotating magnetosphere of **B** exerts a torque on **B** which is larger than the relativistic torque that would be present if **B** were isolated, essentially because the magnetopause radius R_m is small compared to $R_{\rm LB}$. This model (equivalent to a propellor-effect torque, but with a physical basis in field

(a) 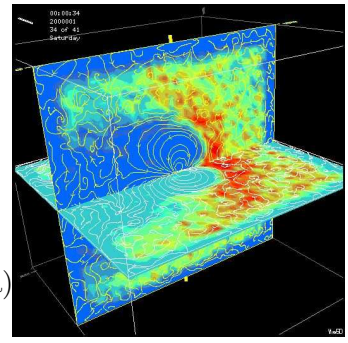 (b) 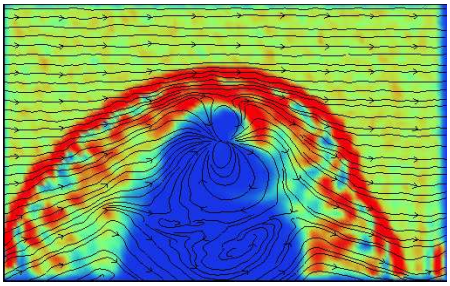

Figure 2. (a) Relativistic 3D PIC simulation of **B**'s rotating magnetosphere immersed in an unmagnetized wind. The magnetospheric obstacle creates a shock heated magnetosheath on the daytime side - the wind approaches from the right. Darker shading indicates the higher density regions in the magnetosheath. Partial trapping of plasma in the cusp creates an asymmetric density structure, with excess plasma in the magnetosheath's afternoon sector. (b) Relativistic 3D PIC simulation of **B**'s rotating magnetosphere immersed in a *magnetized* wind - a snapshot of the equatorial plane. The magnetic field structure shown is in the half period of **B**'s rotation when the wind's and **B**'s magnetic fields are oppositely directed. Reconnection causes field lines to cross the magnetospheric boundary, creating tangential drag on **B**'s magnetosphere, which leads to the dominant torque on **B**. Note the high density region over the polar cusp at "3 o'clock." In the alternate half period, the upstream magnetosphere is closed, with magnetospheric structure similar to the equatorial plane of (a).

dynamics well known from geophysical magnetopsheres) yields the torque

$$\begin{aligned}(\dot{J}_B)_{rec} &\approx -\frac{1}{3}\,\frac{\dot{E}_A \sin^2\Theta_{AB}}{a^2 c}\,\frac{\Omega_B R_{m0}}{c}\,R_{m0}^3 \\ &\approx \left(\frac{\dot{E}_A \sin^2\Theta_{AB}}{a^2 c}\right)^{1/3} \mu_B^{4/3}\,\frac{\Omega_B}{c} \qquad (2) \\ &= 3.3\times 10^{30}\,\mu_{B,30}^{4/3}\,\sin^{2/3}\Theta_{AB}\ \text{erg}.\end{aligned}$$

Using (2) and writing $\dot{E}_B = -\Omega_B \dot{J}_B$ yields $\mu_B = 0.375\times 10^{30}$ cgs ($B_{pole} = 2\mu_B/R_*^3 = 0.75\times 10^{12}$ Gauss), about a factor of 3 less than the value of **B**'s magnetic moment found by Lyne et al. (2004), who used the standard relativistic torque for an isolated RPP to estimate the equatorial surface field of **B**. The torque due to a relativistic wind from **B** (which must flow out the tail, the only region with enough room to allow **B**'s rotation to wind up the magnetic field) is less than 25% of the torque due to dayside reconnection.

3. Synchrotron Absorption in the Magnetosheath

Existing relativistic shock theory (Kennel & Coronoti 1984a; Lyutikov 2004) allows us to evaluate the properties of the shocked magnetosheath plasma at the nose of the magnetosphere, where the shock and the magnetic field are transverse

to the flow. The upstream pair density in the wind is $n_{1\pm} = \mu_A \kappa / 4 P_A e c R_{LA} a^2 = 0.023\kappa$ cm^{-3}, while the upstream magnetic field is $B_1 = \mu_A / 2 R_{LA}^2 a = 6.3$ Gauss, with corresponding cyclotron frequency $\nu_{g1} = 18$ MHz. Currently popular pair creation models suggest $\kappa \sim 10 - 100$ when applied to **A**.

The eclipse profile exhibited by pulsar **A** requires the obscuring plasma to form a belt lying in the plane formed by the line of sight as it passes over (under) pulsar **B** with impact parameter b. The 30 second eclipse duration around superior conjunction corresponds to a belt length 18,600 km, oriented in the direction of the pulsars' relative motion (Kaspi et al. 2004). The light curve of the B pulsar shows a period of $\sim 90^\circ$ in orbital phase centered somewhat before inferior conjunction when B almost disappears (Ramachandran et al. 2004).

We suggest these eclipses are natural consequences of the absorption in the magnetosheath enfolding pulsar **B** — at superior conjunction, the observer looks up the optically thin magnetotail through the absorbing magnetosheath toward **A**, as shown in Figure 1(b), while for a wide range of orbital phase around inferior conjunction, the magnetosheath absorbs **B**'s pulsed radiation along the line of sight to the observer, as is apparent from Figure 1(a). This interpretation implies the absorption to be confined to an apex cap on **B**'s magnetopause, which extends from the magnetospheric axis out to a colatitude of $\theta_{ec} \sim 45^\circ$ from that axis. The simulations shown in Figure 2 are roughly consistent with an absorbing cap of this size. Elementary geometry applied to the solution shown in Figure 1(c), with the length of **A**'s eclipse specified to be 18,600 km, then yields $b = 47,900$ km $= 0.16$ lt-sec, for magnetospheric scale $R_{m0} = 48,400$ km (expression 1) and shock standoff distance at the beginning and end of the eclipse $\Delta_s \approx R_m(\theta_{ec})\beta_2$. This impact parameter corresponds to our view of the system being 3.2° off the orbital plane, or $i = 86.8^\circ$, a value consistent with the measured $i = 87^\circ \pm 3^\circ$.

The asymmetry in the plasma density apparent in Figure 2 is a candidate to explain the asymmetry in the **A** eclipse only if **B**'s rotation is prograde with the orbital motion.

We assume the bow shock converts flow energy into isotropic non-thermal particle distributions with the power law form in given by $N_{2\pm}(\gamma) = (s-1) n_{2\pm} \gamma^{-s}$, with $s > 2$ and $\gamma \geq \gamma_m$. The MHD shock jump conditions yield the post shock temperature T_2, density $n_{2\pm}$ and velocity β_2, all functions of $\sigma = B^2 / 4\pi m_\pm n_{1\pm} \gamma_{wind}$ just upstream of the shock. The post-shock temperature specifies $\gamma_m = (s-2) T_2 / (s-1)$. We assume $\gamma_{wind} = \sigma_0 / (1+\sigma)$, where $\sigma_0 = (B^2 / 4\pi m_\pm n_\pm)_{r=R_{\rm LA}} = 7.5 \times 10^7 / \kappa$.

Standard results for the synchrotron opacity yield the optical depth through the magnetosheath at the apex, where we take the magnetosheath thickness to be $R_{m0}\beta_2$, scaling found in the terrestrial bow shock (Spreiter et al. 1966) and also found in our relativistic simulations. Figures 3(a) and (b), constructed for the case $s = 3$, show that optical depth at 1429 MHz adequate to explain the eclipses of **A** and **B** requires high density in **A**'s wind, $\kappa \approx 10^6$, and low wind magnetization, $\sigma \approx 0.1$. Non-thermal emission from the magnetosheath might be detectable. At high frequencies the magnetosheath becomes optically thin, with emission spectrum varying in proportion to $\nu^{-(s-1)/2}$; at low frequency $f_\nu \propto \nu^{5/2}$. These frequency dependencies neglect the local inhomogeneity of the

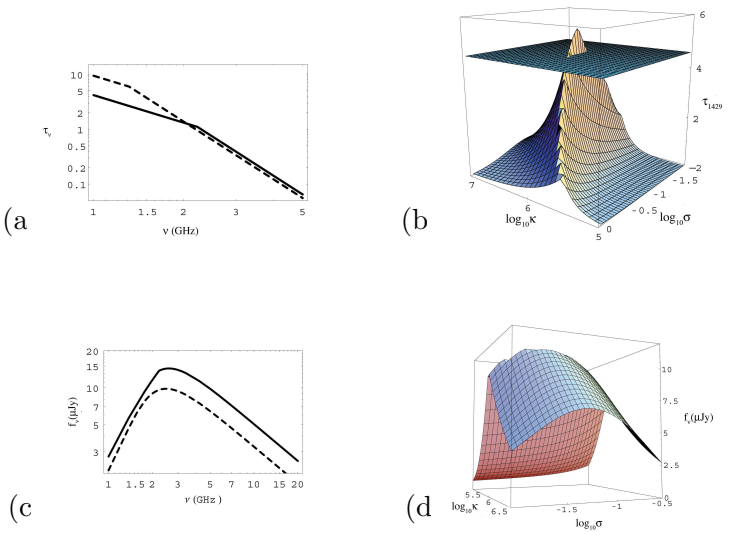

Figure 3. (a) Non-thermal optical depth through the apex magnetosheath as a function of ν for the models with maximum non-thermal magnetosheath emission (solid curve), $\kappa = 10^6$, and $\sigma = 0.03$; minimum density consistent with the eclipse of pulsar **A** at 1429 MHz (long-dashed curve), $\kappa = 10^6$, and $\sigma = 0.2$. (b) Non-thermal optical depth at 1429 MHz as a function of wind density parameter κ, and of wind σ just upstream of the bowshock. The level plane corresponds to optical depth 4.6 (flux at eclipse center 1% of the unobscured flux). (c) Non-thermal synchrotron spectra of the magnetosheath as a function of ν for the models with maximum magnetosheath emission (solid curve), $\kappa = 10^6$, and $\sigma = 0.03$; minimum density consistent with the eclipse of pulsar **A** at 1429 MHz (long-dashed curve), $\kappa = 10^6$, and $\sigma = 0.2$. (d) Non-thermal synchrotron spectra at 2 GHz as a function of density parameter κ and of wind σ. These figures assume a nonthermal particle distribution with $s = 3$ (optically thin emission $\propto \nu^{-1}$), the distance to the pulsars to be 500 pc, a nose radius $R_{m0} = 48,400$ km, and the emitting region to occupy a cap on the apex of the magnetopshere with opening angle 45°.

magnetosheath obvious in Figure 2(b). Figure 3(c) shows the emission spectra for models corresponding to enough optical depth to explain the **A** eclipse, and to yield the maximum emission from the magnetosheath, while Figure 3(d) shows the dependence of the emission flux at 5 GHz on upstream density and on σ.

4. Discussion and Conclusions

Our results show that if synchrotron absorption in the magnetosheath is the cause of eclipse phenomena in this fascinating system, the wind from **A** at latitudes outside the equatorial current sheet ($|\lambda| > 5°$) is dense ($\kappa \sim 10^6$), slow ($\gamma_{wind} \sim 75$) and weakly magnetized at $r \approx 850,000$ km from **A**. The magnetosheath synchrotron absorption model predicts the eclipses will clear at higher frequencies (nominally, $\nu > 5$ GHz), and that synchrotron emission

(probably with some orbital modulation) will be detectable at the level of 5–$10\,\mu$Jy at $\nu \sim 5\,$GHz.

If this is the correct interpretation of the eclipse phenomena, the eclipses are the first (semi-)direct detection of a RPP's wind outside of the equatorial current sheet. Essentially all the phenomena in the young PWNe can be ascribed to the equatorial winds (Kennel & Coroniti 1984a,b; Coroniti 1990; Gallant & Arons 1994; Bogovalov & Khangoulian 2002; Lyubarsky 2002; Komissarov & Lyubarsky 2003, 2004; Spitkovsky & Arons 2004; Del Zanna et al. 2004) as they interact with the plasma of the surrounding PWNe. The density parameter κ is very high compared to expectations derived from current models of magnetospheric pair creation. These have been reasonably successful in accounting for the plasma fluxes inferred to be in the equatorial winds, where we see the results of a very high γ_{wind} outflow. They have not been successful in accounting for the larger populations of lower energy particles which produce the radio synchrotron emission from the young PWNe. The low energy particle injection rates averaged over the history of these systems are factors of 50, and more, larger than derived from standard pair creation models (polar cap, outer gap, slot gap, ...). Our results, and analogous results found by Lyutikov (2004), are even more radical — standard pair creation models applied to **A** yield pair injection rates at least 4 orders of magnitude smaller ($\kappa < 100$) than are required by the magnetosheath synchrotron absorption model.

One solution to the excess low energy plasma problem in young PWNe has been unusual evolutionary spindown history. If the energizing pulsars had much larger spin rates (or magnetic fields) early in their lives than one derives from a constant braking index, constant magnetic moment model, the pair production rates at earlier times might have been much larger, and the equatorial winds much slower, than they are at present. This is a possible (if perhaps unlikely) resolution of the problem, since radio emitting electrons and positrons in the PWNe live "forever," with synchrotron lifetimes much in excess of the PWNe ages.

Such an evolutionary solution cannot explain the plasma overdensity inferred here for **A**'s wind — plasma striking **B**'s magnetosphere emerged from **A** only 3 seconds before it enters the magnetosheath, and flows out of the magnetosheath even more quickly, after absorbing pulsed radiation both from **A** and from **B**. The most efficient explanation of the discrepancy is that the standard pair creation theories are inadequate (i.e., *wrong*), as applied to field lines which feed the non-equatorial wind. We point out that where pair creation models have worked reasonably well, they apply to the feeding of the equatorial wind, and to the origin of pulsed gamma rays — both phenomena occur on field lines connected to the stars near the boundary between the closed and open field lines of their magnetospheres.

Following Ruderman & Sutherland's (1975) vacuum gap model of polar cap pair creation, all subsequent theories have assumed an electrostatic gap structure (strictly steady in the co-rotating frame), with pair plasma taking on the role of poisoning the gap accelerator as fast as the density builds up. The spatial rate of such build up varies, depending on gap geometry and dominant gamma ray emission and pair creation processes, but in all cases, the production rates

required by radio observations are not achieved. In the case of pulsar **A**, one can readily show that if one gives up the concept of gap poisoning and simply asssumes that particle acceleration along the magnetopsheric magnetic field continues uninihibited by pair creation, as in Tademaru's (1973) early cascade model, pair outflows from **A** as large as we have infered from the magnetosheath absorption model are possible. The physics behind such behavior remains to be elucidated.

The PSR J0737−3039 **A** & **B** system clearly has promise for helping us to unravel the mysteries of relativistic outflows from compact objects, as well as providing fascinating phenomenological food for thought and further study. The details of the model described here, along with a number of aspects not touched on in this brief report, will be reported elsewhere.

References

Arons, J. 1998, Mem. Soc. Ast. It., 69, 989

Arons, J. 2002, in Neutron Stars in *Supernova Remnants*, ed. P. O. Slane & B. M. Gaensler (San Francisco: ASP), 71

Arons, J. 2004, Adv. Sp. Res., 33, 466

Arons, J., & Tavani, M. 1993, ApJ, 403, 249

Beskin, V., Kuznetsova, I., & Rafikov, R. 1998, MNRAS, 299, 341

Burgay, M., et al. 2003, Nature, 426, 531

Bogovalov, S. 1999, A&A, 349, 1017

Bogovalov, S., & Khangoulian, D. 2002, MNRAS, 336, L53

Chevalier, R. 2002, in Neutron Stars in *Supernova Remnants*, ed. P. O. Slane & B. M. Gaensler (San Francisco: ASP), 125

Chevalier, R. 2004, Adv. Sp. Res., 33, 456

Contopulos, I., Kazanas, D., & Fendt, C. 1999, ApJ, 511, 351

Coroniti, F. V. 1990, ApJ, 349, 538

Del Zanna, L., Amato, E., & Bucciantini, N. 2004, A&A, 421, 1063

Demorest, P., et al. 2004, ApJ, 615, L137

Fruchter, A., et al. 1988, Nature, 333, 237

Gallant, Y. A., & Arons, J. 1994, ApJ, 435, 230

Gold, T. 1968, Nature, 218, 731

Goldreich, P. & Julian, W. H. 1969, ApJ, 157, 869

Harding, A. K., & Muslimov, A. 1998, ApJ, 508, 328

Hibschman, J., & Arons, J. 2001, ApJ, 560, 871

Hirotani, K, Harding, A. K., & Shibata, S. 2003, ApJ, 591, 334

Johnston, S., et al. 1996, MNRAS, 279, 1026

Johnston, S., et al. 2001, MNRAS, 326, 643

Kaspi, V., et al. 1995, ApJ, 453, 424

Kaspi, V., et al. 2004, ApJ, 613, L137

Kennel, C. F., & Coroniti, F. V. 1984a, ApJ, 283, 694

Kennel, C. F., & Coroniti, F. V. 1984b, ApJ, 283, 710

Komissarov, S., & Lyubarsky, Y. 2003, MNRAS, 344, L93

Komissarov, S., & Lyubarsky, Y. 2004, MNRAS, 349, 779

Lyne, A., et al. 2004, Science, 303, 1153
Lyubarsky, Y. 2002, MNRAS, 329, 34
Lyutikov, M. 2004, MNRAS, 353, 1095
Muslimov, A., & Harding, A. K. 2003, ApJ, 588, 430
Ostriker, J. P., & Gunn, J. E., 1969, ApJ, 157, 1395
Pacini, F. 1967, Nature, 216, 567
Ramachandran, R., et al. 2004, ApJ, in press.
Reynolds, S. 2003, astro-ph/0308483
Ruderman, M., & Sutherland, P. 1975, ApJ, 196, 51
Ruderman, M., et al. 1989, ApJ, 336, 507
Slane, P. 2002, in Neutron Stars in *Supernova Remnants*, ed. P. O. Slane & B. M. Gaensler (San Francisco: ASP), 165
Spitkovsky, A., & Arons, J. 2004, ApJ, 603, 609
Spreiter, J. R., Summers, A. L., & Alksne, A. Y. 1966, Planet. Sp. Sci. 14, 223
Tademaru, E. 1973, ApJ, 183, 625
Tavani, M. & Arons, J. 1997, ApJ, 477, 439
Vlahakis, N. 2004, ApJ, 600, 324